Tribology International 191 (2024) 109102

Contents lists available at ScienceDirect

Tribology International

journal homepage: www.elsevier.com/locate/triboint

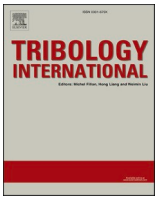

Contribution of viscous shear to friction in cold rolling of low-carbon steel

L.J.M. Jacobs [a,b,*], J. van der Lugt [a], M.B. de Rooij [b]

[a] Tata Steel, Research & Development, IJmuiden, the Netherlands
[b] Chair of Surface Technology & Tribology, Department of Mechanics of Solids, Surfaces & Systems (MS3), Faculty of Engineering Technology, University of Twente, Enschede, the Netherlands

ARTICLE INFO

Keywords:
Cold rolling
Low carbon steel
Lubrication
Modelling

ABSTRACT

This work shows that for temperatures, pressures and shear rates that are common in cold rolling of low-carbon steel, viscous shear stress significantly contributes to the total friction force. Experiments were carried out to validate the theory on lubricant film formation and elasto-hydrodynamic lubrication, both with laboratory scale tribometers and a semi-industrial pilot mill facility. These experiments showed that at high shear rates, that are common in cold rolling, the lubricant does not behave as a Newtonian fluid anymore; moreover the viscosity at high pressure cannot accurately be described by a simple exponential law. With the correct relations implemented in a rolling model, both rolling force and forward slip are predicted with good accuracy for hydrodynamically lubricated cold rolling experiments.

1. Introduction

Rolling is a time and cost-efficient process to reduce the thickness of steel sheet material and is used in the steelmaking industry worldwide. Due to its industrial interest and importance, it is the subject of many studies. The impact of friction on the cold rolling process is well known: because of frictional shear stress, the hydrostatic pressure changes in the rolling contact which results in a non-uniform pressure distribution over the contact length. To underline the root cause, this non-uniform stress distribution is also called the “friction hill”. In the last decades, improved control of friction in cold rolling has led to improvement in strip quality, higher productivity and a decrease of rolling costs. Therefore, according to Roberts [1]: "*Of all the variables associated with rolling, none is more important than friction in the roll bite … its control within an optimum range for each process is essential*". Research into this subject is still very relevant, recent research works focus on the influence of friction on mill stability (Heidari et al. [2] or Lu et al. [3]), strip cleanliness (Mekicha et al. [4] or Montmitonnet et al. [5]), rollability of hard steel grades (Shimura et al. [6] or Wu et al. [7]), modelling of lubrication mechanisms (Boemer [8]), lubricant testing (Smeulders [9]) and new lubricant application methods (Bergmann et al. [10] or Laugier et al. [11]).

The relevant friction mechanisms in a lubricated contact between rough surfaces (such as the roll bite) are adhesion, ploughing and viscous shear (Bushhan [12]). A precise quantification of these frictional forces in cold rolling enables to calculate the exact shape of the friction hill and therefore enables a better simulation of the cold rolling process.

Von Karman lay the basis of the so called ‘slab-model’ to calculate the pressure distribution in cold rolling [13]. At first, the role of the lubricant was not considered explicitly and dry sliding was assumed between work roll and strip material, described by the Coulomb friction law. Compared with Coulombs law for sliding friction, other formulations for the frictional force in the roll bite lead to a less steep friction hill (Roberts [14]).

Nadai [15] was the first to explicitly take the effect of lubricant into account in his rolling model. Later, more physically based friction models came in use, whereby the friction depends explicitly on the lubricant film thickness that is entrained in the roll bite. For a hydrodynamic lubricated rolling process, this led to the well-known film thickness equation by Wilson and Walowit [16], or to a fully hydrodynamic cold rolling model by Lugt [17]. As cold rolling is best performed in the mixed lubrication regime, the next step was the development of mixed-lubrication models. Marsault [18] describes a complete mixed-lubrication model for cold rolling. In the last decades, these models were developed further; the work of Boemer [8] appears to be the current state-of-the-art regarding modelling of the mixed lubrication regime for cold rolling.

In such physically based friction models, the lubricant properties become important as they determine (together with the process, strip and work roll parameters) the lubricant film thickness and the viscous

* Corresponding author at: Tata Steel, Research & Development, IJmuiden, the Netherlands.
E-mail address: leon.jacobs@tatasteeleurope.com (L.J.M. Jacobs).

https://doi.org/10.1016/j.triboint.2023.109102
Received 4 September 2023; Received in revised form 6 November 2023; Accepted 8 November 2023
Available online 10 November 2023

shear stress. Viscosity is a key characteristic of the lubricant. Using viscous lubricants results in thicker lubricant layers (Wilson and Walowit [16]) as well as a higher shear stress (for a given film thickness and shear rate). The rate of viscosity increase with pressure is another key characteristic of lubricants. Azushima [19] describes how hydrodynamic lubrication is favoured for lubricants with a high pressure-viscosity coefficient. Furthermore, it is well-known that viscosity decreases significantly with temperature (Azushima [20]).

From the previous it follows that for the purpose of modelling friction in cold rolling, the exact dependence of viscosity with pressure and temperature is important. Many developers of mixed-lubrication models have determined the relevant lubricant properties by fitting their model with experimental rolling results. However, this method is not desirable as it could mask other shortcomings in the model. The current consensus is that these rheological parameters need to be independently determined.

In the last decade there has been an ongoing debate about the preferential experimental method to determine these properties. A direct measurement of viscosity is championed by Bair and co-workers [21,22]. The other method, long-time used 'classical EHL', derives the rheological parameters from experimental traction curves of an EHL contact [23]. The advantages and disadvantages of both methods are discussed in [24–26]. In this work the classical EHL-approach is chosen and the method by Moes [23] is followed to extract the relevant viscosity parameters by fitting experimental elastohydrodynamic lubrication results to theory.

In cold rolling it is generally accepted that viscous shear stresses are smaller than frictional stresses resulting from direct contact between the work roll and strip. Many researchers have used this fact to neglect viscous shear stresses in their mixed lubrication models, but robust experimental results to justify this assumption have so far not been presented in the literature.

Here, the dependence of viscosity with temperature and pressure is determined experimentally for a commercially available rolling oil. Furthermore, it is investigated if the resulting description of viscosity is consistent, both in laboratory scale experiments and in cold rolling experiments, both to determine lubricant film thickness as well as viscous shear stress. Additionally the relative importance of viscous shear is determined and compared to shear stresses caused by direct interaction of the work roll and strip. Finally, the measured viscosity-pressure-temperature relation is integrated in a cold rolling model based on the slab-method, resulting in a rolling model without the necessary input of a coefficient of friction (but purely based on measured material, work roll and lubricant properties). In this study, the accuracy of this rolling model to predict the rolling force and forward slip is evaluated for hydrodynamic lubricated cold rolling processes.

2. Theory

This section describes the theory that is used to analyse the experimental results. The theory related to lubricant viscosity and viscous shear stress is detailed, as well as the cold rolling model that is used to interpret the results from the rolling trials.

2.1. Lubricant viscosity

Lubrication theory took off when Reynolds [27] described how the pressure within a lubricant changes in a converging gap as is the case in the cold rolling process. The lubricant flow in cold rolling can be considered as a one-dimensional steady state process, therefore the original Reynolds Equation can be simplified to a one-dimensional equation:

$$\frac{\partial}{\partial x}\left[\frac{\rho h^3}{\eta}\frac{\partial p}{\partial x}\right] = 6\left(V_{roll}+V_{strip}\right)\frac{\partial(\rho h)}{\partial x} + 6\rho h\frac{\partial\left(V_{roll}+V_{strip}\right)}{\partial x} \tag{1}$$

Where x is the coordinate in the rolling direction, ρ the lubricant density, h the lubricant film thickness, V_{roll} the work roll speed, V_{strip} the strip speed, p the lubricant pressure and finally η is the lubricant's dynamic viscosity. For cold rolling, the Reynolds Equation can be solved numerically as in Marsault [18] with a shooting method or, as in Qiu et al. [28], with a finite difference method to find the lubricant film thickness in the roll bite. Patir and Cheng [29] have shown that the influence of surface roughness can be incorporated with flow factors in the so-called stochastic Reynolds Equation. In Eq. (1) the strip and roll velocity are known from the geometry of the process. The lubricant density depends on pressure (see Dowson and Higginson [30]), but not as much as the lubricant viscosity. Therefore in this work the lubricant will be considered as incompressible and only the influence of pressure and temperature on lubricant viscosity is studied.

Several rheological laws have been proposed to quantify the relation between viscosity, pressure and temperature. A widely used relation is the exponential Barus-equation [31]:

$$\eta(p) = \eta_{p_{atm},T_{ref}}\cdot e^{\alpha\cdot p} \tag{2}$$

where $\eta_{p_{atm},T_{ref}}$ is the dynamic viscosity at atmospheric pressure and reference temperature and α is the viscosity-pressure parameter. Temperature dependence can be easily included, resulting in an extended Barus equation (see for example Azushima [20]):

$$\eta(p,T) = \eta_{p_{atm},T_{ref}}\cdot e^{\alpha\cdot p-\beta\cdot(T-T_{ref})} \tag{3}$$

with T the temperature, T_{ref} the reference temperature and β the viscosity-temperature coefficient.

Based on measurements with a high-pressure viscometer, Roelands [32] presents a more precise description of lubricant viscosity as a function of temperature and pressure. In the simplified Roelands Equation, which is most often cited, there is no interdependence between the influence of pressure and temperature on viscosity:

$$\eta(p,T) = \eta_{p_{atm},T_{ref}}\cdot e^{(\ln(\eta_{p_{atm},T_{ref}})+9.67)\cdot\left\{\left(1+\frac{p}{p_r}\right)^{z}\cdot\left(\frac{T_0-135}{T-135}\right)^{s_0}-1\right\}} \tag{4}$$

Where s_0 is the viscosity-temperature index, z the viscosity-pressure parameter, T_0 the reference temperature (T and T_0 in °C) and p_r a constant with value $1.962{\cdot}10^8$ Pa. In this formula $\eta_{p_{atm},T_{ref}}$ is in Pa·s and the pressure p is in Pa. Even more precise is the so-called extended Roelands equation [32], which accounts for a (small) interdependence of the term related to temperature and the term related to pressure; z in Eq. (4) now becomes an equation of the lubricant temperature:

$$z(T) = D_{ROE} + C_{Roe}\cdot\ln\left(\frac{135}{135+T}\right) \tag{5}$$

Where D_{ROE} and C_{ROE} are two constants that must be determined by fitting Eqs. (4) and (5) with measurements. Other conceptual relations between viscosity, pressure and temperature are also used, such as the physically based WLF-equation (Williams et al. [33]). As will be shown later in this article, the viscosity-pressure-temperature relation of the investigated cold rolling lubricant can be captured accurately enough with the (extended) Roelands equation.

In this work a setup is used where two surfaces, separated by a hydrodynamic lubricant film, are sliding against each other. The viscosity-pressure-temperature relation can be determined because the viscosity relates the viscous shear stress with the shear rate. Often it is assumed that the lubricant behaves as a Newtonian fluid, meaning a proportional relation between viscous shear stress τ_{visc} and shear rate $\dot{\gamma}$:

$$\tau_{visc} = \eta(p,T)\cdot\dot{\gamma} \tag{6}$$

At very high shear rates ($\dot{\gamma} > 10^6\ s^{-1}$), the relation between τ_{visc} and $\dot{\gamma}$ usually becomes non-linear. Bell et al. [34] found that this behaviour

was well described by the Eyring equation:

$$\tau_{visc} = \tau_0(p,T)\cdot\text{asinh}\left(\frac{\eta(p,T)\cdot\dot{\gamma}}{\tau_0(p,T)}\right) \tag{7}$$

Where $\tau_0(p,T)$ is the so called limiting Newtonian shear stress (the stress above which the Newtonian assumption is not valid anymore). This equation was used for example by Sutcliffe [35] in his mixed lubrication cold rolling model; as will be shown later, it also describes well the viscous shear stress of the currently investigated rolling oil. Also other relations between viscous shear stress and shear rate are known, Gelinck [36] provides a good overview of different classes of rheological lubricant behaviour and the relevant models (linear viscous, non-linear viscous, viscoelastic and viscoplastic behaviour). For the lubricant investigated in this work, the Deborah number [37] remains well below 1, hence elastic effects in the lubricant can be neglected compared to the viscous effects. Furthermore, as τ_{visc} continuously increases with $\dot{\gamma}$ in our experiments, it can be concluded that the ultimate strength (or limiting shear strength) of the lubricant has not been reached.

Ball-on-disk instruments are used for the laboratory-scale experiments; the theory developed by Hertz is used to determine the contact radius between ball and disk (Spikes [38]):

$$r_{contact} = \left(3\cdot L\cdot R^{'}/2\cdot E^{'}\right)^{1/3} \tag{8}$$

Where L is the applied load, $R^{'}$ the equivalent radius of curvature (equal to ball radius for a ball-disk contact) and $E^{'}$ the equivalent elastic modulus. With this contact radius, the average pressure and shear stress can be determined from the measured load and frictional force. These average values will be used to determine the viscosity-pressure-temperature relation.

To analyse the experiments, the speed difference of the ball and disk must be converted to a shear rate, therefore the lubricant film thickness must be known. This film thickness is estimated with the well-known formula by Moes [23] which is detailed in the appendix. Although the Moes formula as specified in the appendix is valid for a point contact, it is derived from the more general film thickness equations for an elliptical contact geometry. The pressure-viscosity coefficient is an input parameter of the Moes formula. If Barus equation is assumed, this parameter is equal to α (see Eq. (2)), whereas if Roelands equation (Eqs. (4) and (5)) is assumed this parameter still depends on the pressure. To circumvent this, Blok [39] has defined an 'equivalent pressure-viscosity coefficient' α^* as:

$$\alpha^* = \left\{\int_0^\infty \frac{\eta_{p_{atm},T_{ref}}}{\eta(p)}dp\right\}^{-1} \tag{9}$$

This parameter can be used in the Moes-formula to predict the lubricant film thickness when the lubricant viscosity is described with the (extended) Roelands equation. Moes [23] gives an approximation of α^* for the Roelands equation, expressing α^* in $z(T)$:

$$\alpha^*(T) \approx \frac{\left(\ln\left(\eta_{p_{atm},T_{ref}}\right)+9.67\right)\cdot\frac{z(T)}{p_0}}{1+\frac{1-z(T)}{\left(\ln\left(\eta_{p_{atm},T_{ref}}\right)+9.67\right)\cdot z(T)}} \tag{10}$$

again with $\eta_{p_{atm},T_{ref}}$ in Pa·s.

From the previous it follows that in the analysis of a single ball on disk experiment, the lubricant viscosity is used twice: once in the Moes formula and once to relate viscous shear stress with shear rate. In this research an iterative approach is followed to numerically determine the viscosity (for a given lubricant pressure and temperature), so that the results represent the best fit with the experimental results and they are consistent with both Eq. (7) and Eq. (A.7). A flow chart of this iterative procedure is shown in Figure A1 in the appendix.

2.2. Hydrodynamic cold rolling model

A hydrodynamic rolling model based on the slab method is used to analyse the hydrodynamic cold rolling experiments. According to Montmitonnet [40], for the rolling conditions described in this work, a slab model accurately describes the cold rolling process. The rolling model can be split up in two parts:

1) A model to determine the lubricant flow, primarily in the inlet zone of the contact.
2) A model to describe the deformation of the work roll and strip in the work zone.

Obviously, both parts are strongly coupled because the pressure in the lubricant is regulated by the strip deformation and also because the friction between work roll and strip results from the lubricant film thickness (and its rheological properties). See Fig. 1 for the geometry of the cold rolling process and the definition of the different zones in the contact.

The first part, the model that calculates the lubricant flow, solves the Reynolds Equation (Eq. (1)) in the inlet zone of the roll bite. In this work, the model is not described in detail (see Lugt [17] or Boemer [8] for details), but its main features are highlighted:

- In the inlet zone, the geometry of the converging gap is determined taking into account both elastic work roll deformation (via the Boussinesq approach, Eq. (12)) and elastic strip deformation (via the elastic von Karman equation, [17]). An iteration loop is used to simultaneously solve the elastic deformation and the Reynolds Equation.
- The model uses the viscosity-pressure-temperature relation described by the extended Roelands equation (Eqs. (4) and (5)) with fit parameters determined in this work.
- The influence of strip and work roll roughness on lubricant flow in the rolling process is taken into account by flow factors [29,41]. The used flow factors are based on Gaussian distributed roughness characterised by a Peklenik number [42] of 9, representing the longitudinal lay of the ground work roll surface.
- The lubricant temperature is the average of the work roll temperature and strip temperature, which are both assumed to be constant in the inlet zone.
- Contrary to Lugt [17], the 1D Reynolds Equation is solved with a Finite Difference method, similar as in Cassarini [43].

In this way, the lubricant film thickness at the entry of the roll bite is obtained. When the rolling process is in the hydrodynamic lubrication regime, the film thickness anywhere in the roll bite can then be deduced from mass conservation of the lubricant:

$$h(x) = h_{entry}\cdot\frac{v_{strip,entry}+v_{roll}}{v_{strip}(x)+v_{roll}} \tag{11}$$

where $h(x)$ is the lubricant film thickness at position x in the roll bite, $v_{strip}(x)$ is the strip speed at that position, h_{entry} is the lubricant film thickness at the entry of the roll bite as determined from the model and $v_{strip,entry}$ is the strip speed at the entry of the roll bite. As the pressure gradient in the work zone is small, it is assumed that any backflow of lubricant can be neglected [16].

The second part of the model describes the mechanics of strip and work roll. Again, this part of the model is not described in detail (see Montmitonnet [40]), but again its main features are highlighted here:

- The material work hardening behaviour is modelled as described by Van Liempt [44]. The Hill48 yield criterion [45] is used to take anisotropic yielding behaviour into account. The relevant mechanical properties for the materials used in the experiments, yield stress

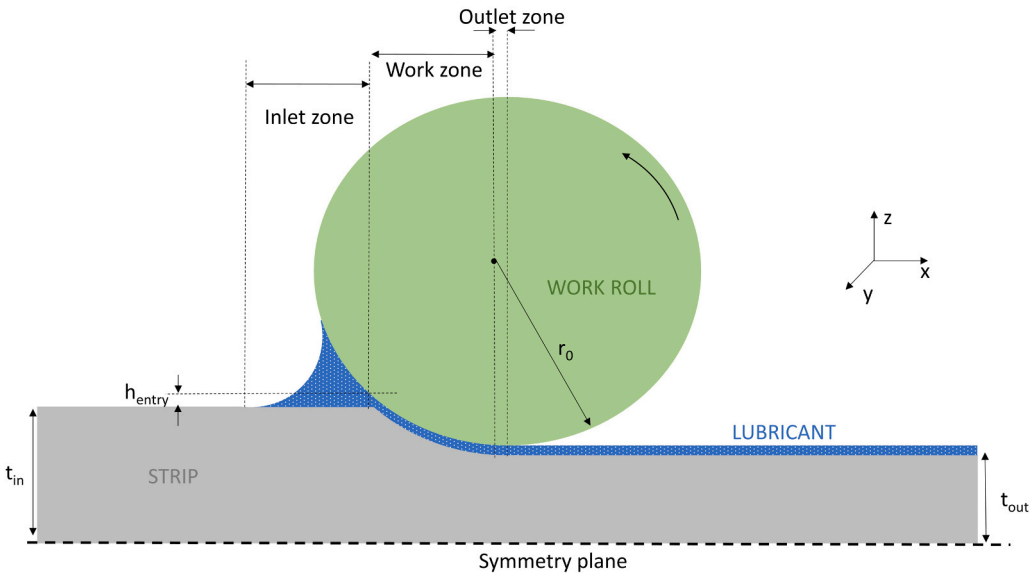

Fig. 1. geometry of cold rolling process; division of contact zone in inlet zone, work zone and outlet zone.

and the Lankford parameter R_0, were measured by Jacobs et al. [46] and are reproduced in Fig. 5.

- Work roll flattening defines the strip thickness in each segment. Based on the local strip thickness, the local strip speed can be determined by considering mass conservation of the strip. For cold rolling, usually elastic work roll deformation is described by the Hitchcock equation [47]. In this work, some rolling experiments were carried out with very small thickness reduction. This results in a small bite angle, which helps to approach pure hydrodynamic lubrication conditions during rolling. For such rolling processes Hitchcock is not a valid assumption. Then, elastic deformation of the work roll can be obtained by a Boussinesq approach, so by integration of the deformation caused by point forces representing the contact pressure distribution, as for example described by Johnson [48]:

$$w(x) = -\frac{2(1-\upsilon^2)}{\pi E}\int_{-\infty}^{\infty} p(s)\ln\left|\frac{x-s}{x_0-s}\right| ds + c \tag{12}$$

Where c is an integration constant. Lugt [17] shows that this equation can be discretized as follows:

$$w(x_i) = -\frac{2(1-\upsilon^2)}{\pi E}\sum_{j=1}^{n} K_{ij} p_j \tag{13}$$

Where $K_{ij} = (i-j+0.5)\Delta(\ln(|i-j+0.5|)\Delta - 1) - (i-j-0.5)\Delta \quad (\ln(|i-j-0.5|)\Delta - 1$ and Δ is the grid size.

- At the end of the roll bite, an elastic recovery zone is integrated in the model.
- Usually in slab models, the Coulomb friction law is used. In this work a physically based friction law for hydrodynamic conditions is used, based on the measured lubricant properties. The lubricant film thickness at the entry of the roll bite is calculated in the first part of the model, Eq. (11) is used to determine the lubricant film thickness in the rest of the roll bite. With the lubricant film thickness the shear rates can be determined and the viscous shear stress in each element is determined with Eq. (7).
- Heat is generated during the rolling process because of plastic deformation and friction. An adiabatic model is used, the generated heat in one segment is distributed uniformly over the strip in that segment. The lubricant temperature is taken equal to the average of the local strip temperature and the isothermal work roll temperature.

The main outputs of the complete rolling model are the lubricant film thickness, the rolling force and the forward slip (defined as: $(V_{strip}/V_{roll} - 1)\cdot 100\%$), which can be compared to the values measured in the experiments.

3. Experimental set up

One objective of this work is to characterise the viscosity-pressure-temperature relation of a commercially available cold rolling oil, with the underlying goal of implementing this relation in the cold rolling model. The rolling oil that is used for this investigation is TotalEnergies RK1832DR, a rolling oil typically used in a Double Cold Rolling mill. The dependence of dynamic viscosity with temperature, at atmospheric pressure, is shown in Fig. 2. The best fit with the Roelands equation is obtained with values for $\eta_{p_{atm},T_{ref}}$ of 0.03245 Pa·s at 40 °C and the temperature-viscosity coefficient s_0 of 1.031, the resulting fit is also shown in Fig. 2. The dependence of viscosity with pressure for RK1832DR is determined in the experiments described in Section 3.1.

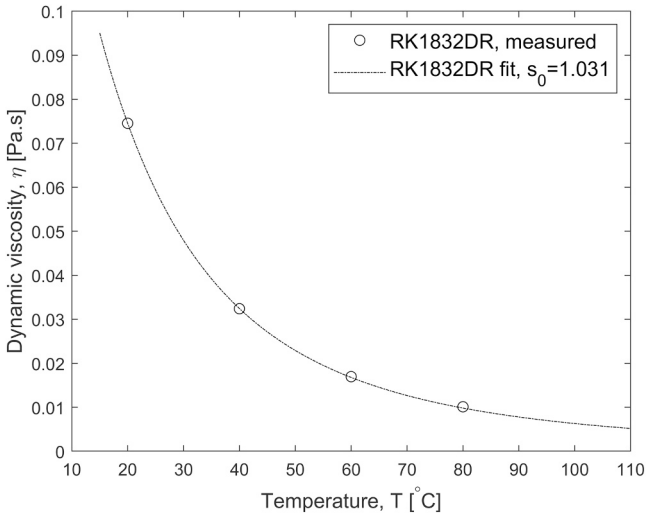

Fig. 2. viscosity-temperature relation for RK1832DR at atmospheric pressure.

3.1. Ball-on-disk experiments

The laboratory-scale experiments were carried out on two different ball-on-disk instruments at TotalEnergies laboratory. The MTM (Mini Traction Machine) was used to measure the viscous shear stress and deduce from that the viscosity as function of pressure and temperature. The EHL-rig (ElastoHydrodynamic Lubrication rig) was employed to directly measure the lubricant film thickness, which can be used to validate the measured viscosity obtained on the MTM. Both machines are commonly used for experimental tribological research, a schematic overview is shown in Fig. 3.

The MTM can be used to study the frictional behaviour in all three lubrication regimes (boundary, mixed and elasto-hydrodynamic), but in this work only hydrodynamic lubrication is considered. The R_a-value of both ball and disk are approximately 10 nm, so that the process is in the hydrodynamic lubrication regime for lubricant films thicker than 50 nm. The used MTM accessories are a 19.05 mm diameter steel ball and a 46 mm diameter steel disc. The experiment is setup by loading the ball against the flat surface of the disc at an inclined axis to prevent spin within the contact. Ball and disk are placed in a steel pot to which approximately 50 ml of lubricant is added, so that the contact is immersed in lubricant. Ball and disk are then driven separately, allowing to achieve any ratio of rolling and sliding speed.

During a single MTM-experiment, the pressure and temperature are controlled at the set values. Furthermore the sum speed (ball speed + disk speed) remains constant so that, according to the theory, the lubricant film thickness remains constant (see for example the Moes equations in the Appendix). It was experimentally verified that the viscosity, as deduced from the MTM-experiments, is independent of the chosen sum speed. For the experimental results presented in this work, all MTM-trials were carried out at a sum speed of 1 m/s. By changing the relative speed of ball and disk, the shear rate in the lubricant film is varied (up to 10^7 s^{-1} approximately). The frictional force is continuously measured and can be related to this shear rate, from which the viscosity (at that specific temperature and pressure) can be determined as outlined in Section 2. The methodology is also well described by Spikes [38].

Such experiments were repeated for a range of lubricant temperatures and pressures. Table 1 gives an overview of all test conditions together with the relevant material properties and dimensions of ball and disk. The achieved range in shear rate, temperature and pressure covers almost the entire range that is common in the cold rolling of low-Carbon steel.

The EHL-rig can be used to directly measure lubricant film thickness in the elastohydrodynamic lubrication regime. The used EHL accessories are a 19.05 mm steel ball and a highly reflective glass disk. Roughness of both surfaces is low: the ball has an R_a-value of 15 nm and the disk an R_a-value of 5 nm, so that for film thickness higher than approximately 70 nm the process is in the hydrodynamic lubrication regime. The experiment is setup by adding 120 ml of lubricant to the reservoir and then heating it up to the desired temperature; the ball must be half immersed in lubricant. Once the load is set, the microscope and spectrometer are adjusted to obtain a clear spectral image of the contact. To avoid damaging the disk, the ball and disk speeds are kept equal throughout the experiment.

Table 1
overview of process conditions and disk/ball properties of MTM-experiments.

Parameter	Value
Ball diameter [m]	0.01905
R_a-value ball/disk [m]	$1{\cdot}10^{-8}$
Youngs modulus ball/disk [Pa]	$2.07{\cdot}10^{11}$
Poisson ratio ball/disk [–]	0.29
Sum speed [m/s]	1
Applied Force [N]	2.5, 5, 10, 20, 30, 40, 50
Lubricant Temperature [°C]	40, 60, 80, 110, 150

During a single EHL-experiment, the pressure and temperature are controlled at the set values. By increasing the speed of ball and disk, the lubricant film increases as well. The lubricant film thickness is continuously measured by optical interferometry method whereby the focused white light is reflected from two areas: the reflective chromium layer in the disc and the steel ball. The methodology is also well described by Van Leeuwen [50]. Such experiments were repeated for other lubricant temperatures. Table 2 gives an overview of all test conditions together with the relevant ball and disk material properties and dimensions.

3.2. Rolling experiments

The rolling experiments are carried out on the Tata Steel pilot mill, see Fig. 4 for a photo and a schematic presentation.

In these experiments, the stand-alone mill operates in a two-high configuration (i.e. without backup rolls). The work rolls have a diameter of 397 mm and a ground roughness with an R_a-value of 0.07 μm. Entry and exit tension are generated by the uncoiler and coiler.

The materials that were used in the trials are 100 mm wide tinplate grades. The mechanical properties were measured by Jacobs et al. [46] and are reproduced in Fig. 5. Fig. 5a shows the measured yield stress at

Table 2
overview of process conditions and disk/ball properties of EHL-experiments.

Parameter	Value
Ball diameter [m]	0.01905
Ball Ra-value [m]	$1.5{\cdot}10^{-8}$
Disk Ra-value [m]	$5{\cdot}10^{-9}$
Youngs Modulus Ball [Pa]	$2.07{\cdot}10^{11}$
Youngs Modulus Disk [Pa]	$7.5{\cdot}10^{10}$
Poisson Ratio Ball [–]	0.29
Poisson Ratio Disk [–]	0.22
Applied Force [N]	20
Range Speed [m/s]	0.03 – 3
Lubricant Temperature [°C]	20, 40, 60, 80

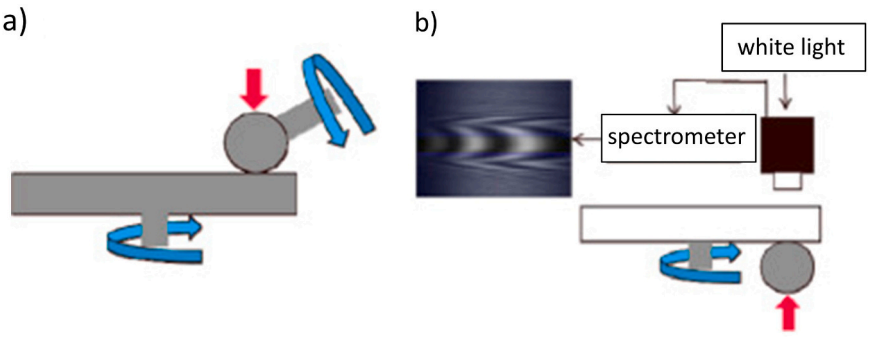

Fig. 3. a) schematic overview of MTM, b) schematic overview of EHL-rig, both figures adapted from De Laurentis et al. [49].

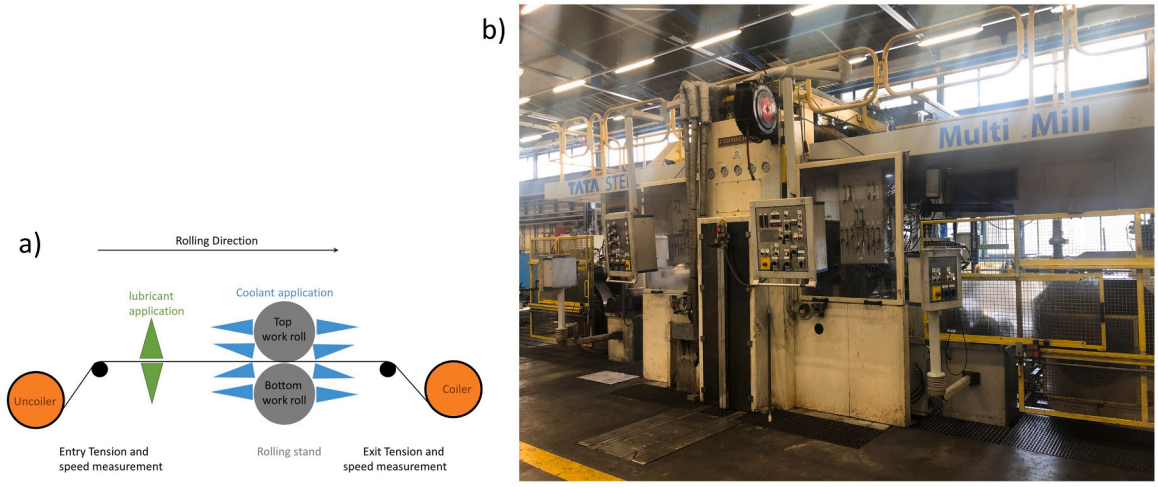

Fig. 4. a) schematic layout of the pilot mill, b) photo of the pilot mil.

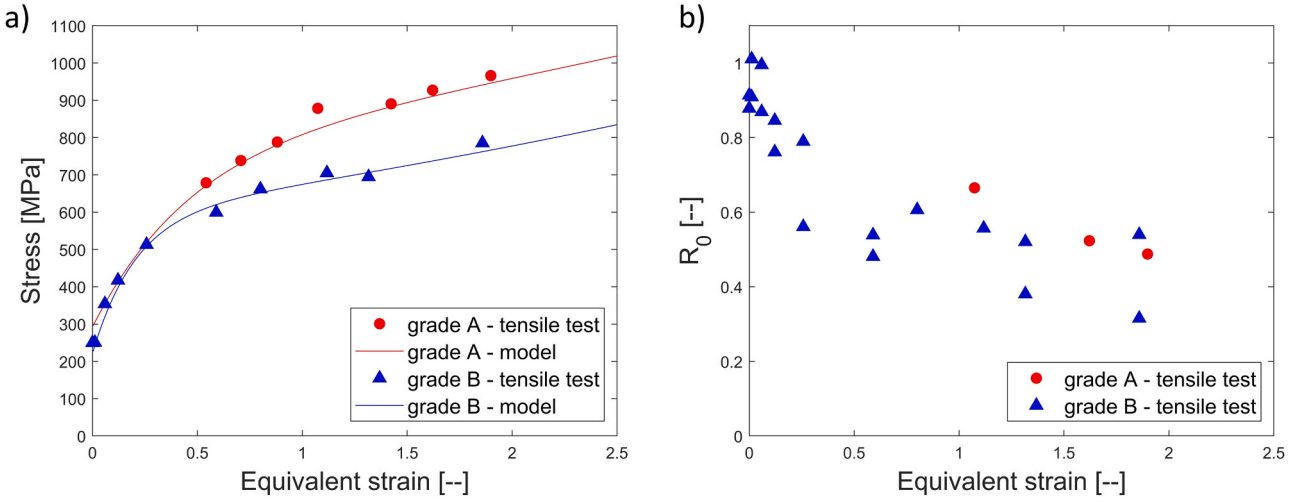

Fig. 5. a) stress-strain curve of the material used in the pilot mill trials; the markers are tensile test results at a strainrate of 0.01 s^{-1} (each datapoint is the average of 2–4 tensile tests), the lines are results of the constitutive model as implemented in the rolling models (at strain rate of 0.01 s^{-1}). b) Lankford parameter in rolling direction as measured by the tensile tests (each datapoint is a separate measurement).

various level of equivalent strain, as well as the fit with the material model described by Van Liempt [44]. This constitutive model takes viscoplastic effects into account, all results shown in Fig. 5 are obtained at a strain rate of 0.01 s^{-1}. The same model is implemented in the cold rolling models that are used to analyse the rolling trials. Fig. 5b shows the Lankford parameter in rolling direction as function of equivalent strain; Jacobs et al. [46] show that this parameter has a significant influence on the cold rolling force.

Two types of cold rolling experiments were carried out: droplet trials and hydrodynamic lubrication trials. The oil droplet method was first used by Saeki and Hashimoto [51] and described by Azushima [52]. A droplet of oil with a known volume is placed with a calibrated pipette on the strip before rolling. During rolling, the droplet is rolled out to an ellipse-shaped spot on the strip, the surface area of the spot is estimated by measuring the length of the two principal axes of the ellipse. The average lubricant film thickness at the exit of the roll bite is then determined as the quotient of the known droplet volume and the measured surface area of the spot after rolling.

The volume of the applied droplet must be exactly known. Therefore, any oily residues on the strip must be removed prior to rolling. In our tests, the entire coil is degreased before each pass; the spot where the droplet is placed is further cleaned manually with acetone. All relevant process details of the droplet experiments are given in Table 3.

Good reproducibility of the droplet trial has been reported (for example by Cuperus et al. [53]), but usually the agreement between experimental results and model results was quite poor. Sutcliffe [35] measured lower lubricant film thickness than his model predictions, while Aggerwal and Wilson [54] measured up to 4 times higher lubricant film thickness than their model predictions. Jacobs et al. [55] found that asymmetric material entrance was the root cause of the discrepancy between theory and experiments. They found a correction factor, to correct the measured lubricant film thickness under asymmetric strip feeding conditions to film thickness for symmetric feeding conditions (which corresponded to model results). In this work the same droplet trials are used to validate the theory and MTM-results, therefore the same correction factor is applied for experiments with asymmetric strip feeding.

Contrary to the droplet trials, the hydrodynamic lubrication trials were carried out by applying an abundance of the lubricating oil RK1832DR. Rolling conditions were chosen to enhance lubricant film formation and rolling in the hydrodynamic regime (i.e. relatively low reduction, high speed and low temperature). These rolling conditions are specified in Table 4. Table 6 presents the calculated film thickness for each experiment, showing that for trial 1A-1D the process is in the

Table 3
process parameters of the droplet trials.

Test Nr.	t_{in} (mm)	t_{out} (mm)	Rolling Force (kN)	Tension In/Out (kN)	R_a strip (micron)	Rolling Speed (m/s)	Average Temp (°C)[a]
1a	1.6	1.41	630	5 / 10	0.4	0.1–0.2–0.4–0.8–1.6	[b]
1b	1.3	1.00	815	5 / 10	0.3	0.1–0.2–0.4–0.8–1.6	[b]
1c	0.7	0.63	700–950–1200	5 / 10	0.1	0.4–1.6	[b]
1d	1.3	1.20	500	5 / 10	0.5	0.2–0.4–0.8	[b]
1e	1.1	1.01	500	5 / 10	0.4	0.2–0.4–0.8–1.6	[b]
2a	1.5	1.37	500	7.5 / 7.5	0.4	0.2–0.4–0.8–1.6	24.3 ± 0.1
2b	1.5	1.24	650	7.5 / 7.5	0.4	0.2–0.4–0.8–1.6	24.0 ± 0.3
3a	0.84	0.76	700	7.5 / 7.5	0.1	0.2–0.4–0.8–1.6	21.8 ± 0.4
3b	0.84	0.80	500	7.5 / 7.5	0.1	0.2–0.4–0.8–1.6	22.2 ± 0.5

[a] *This column shows the average temperature (of roll and strip) of all droplet experiments within that test number.*
[b] *The roll temperature was not measured for these passes. In the model calculations an average temperature of 23°C was assumed, which is the average temperature in the passes where the temperature was measured.*

Table 4
average process parameters of hydrodynamic lubrication trials. The graphs and model simulations in Sections 4 and 5 are based on the actual measured values. Test 1A-1D are carried out with material grade A, test 2A-2E are carried out with material grade B. In test 1A and 1B the rolling speed is varied, in test 1 C and 1D the entry tension is varied (the number of variations is indicated in the table).

Test Nr.	Entry / Exit Thickness (mm)	Entry / Exit Tension (MPa)	Rolling Speed (m/s)	Strip / Roll R_a (μm)	Strip / Roll Temp (°C)
1A	0.95 / 0.89	33 / 111	4 and 6	0.52 / 0.10	35 / 35
1B	0.59 / 0.56	104 / 177	5 and 6	0.39 / 0.10	35 / 35
1 C	0.95 / 0.89	53–105 / 112	6	0.41 / 0.10	36 / 30
1D	0.55 / 0.53	74 and 92 / 189	6	0.35 / 0.10	40 / 34
2A	1.40 / 1.20	42 / 83	6	0.42 / 0.70	21 / 30[a]
2B	1.20 / 1.00	50 / 101	7	0.70 / 0.70	30 / 30[a]
2 C	1.00 / 0.90	59 / 111	7	0.76 / 0.70	30 / 30[a]
2D	0.90 / 0.80	67 / 125	8	0.74 / 0.70	29 / 30[a]
2E	0.66 / 0.50	91 / 199	10	0.78 / 0.70	33 / 30[a]

[a] *Test 2 was cooled with an emulsion at the exit side, with temperature of 30 °C, which kept the roll temperature relatively constant at 30 °C.*

hydrodynamic lubrication regime, while for trial 2A-2E the lubrication is almost hydrodynamic.

4. Results

4.1. Results MTM

A typical result of an MTM-experiment is shown in Fig. 6 where the frictional shear force F_x is plotted as a function of the slide-roll-ratio (SRR) which is defined as SRR $= 2{\cdot}|u_{ball} - u_{disk}|/(u_{ball} + u_{disk})$.

The shear force is converted into a shear stress by dividing the shear force by the Hertzian contact area. The SRR can be converted into a shear rate using the film thickness calculated by Moes-formula. This allows to plot the shear stress vs. shear rate as in the right graph of Fig. 6. The best fit for a Newtonian fluid (Eq. (6)) and the best fit with the Eyring-equation (Eq. (7)) are also shown. That last fit directly yields the viscosity and limiting Newtonian shear stress at the specified temperature and pressure.

Fig. 6 shows that at high shear rates, the viscous shear stress is not accurately predicted with the Newtonian fluid assumption. For even higher shear rates, the shear stress decreases because the lubricant temperature increases as a result of viscous shear heating. This 'thermal regime' is not modelled in any way by Eq. (7) (or Eq. (6)), Fig. 6 shows that the thermal regime was not reached in that experiment.

Analysis has shown that with this fitting procedure, $\eta(p, T)$ can be determined from the MTM-measurements with an accuracy better than 5%.

The procedure to obtained viscosity and limiting Newtonian shear stress from the measurements (as detailed in Section 2.1) was carried out

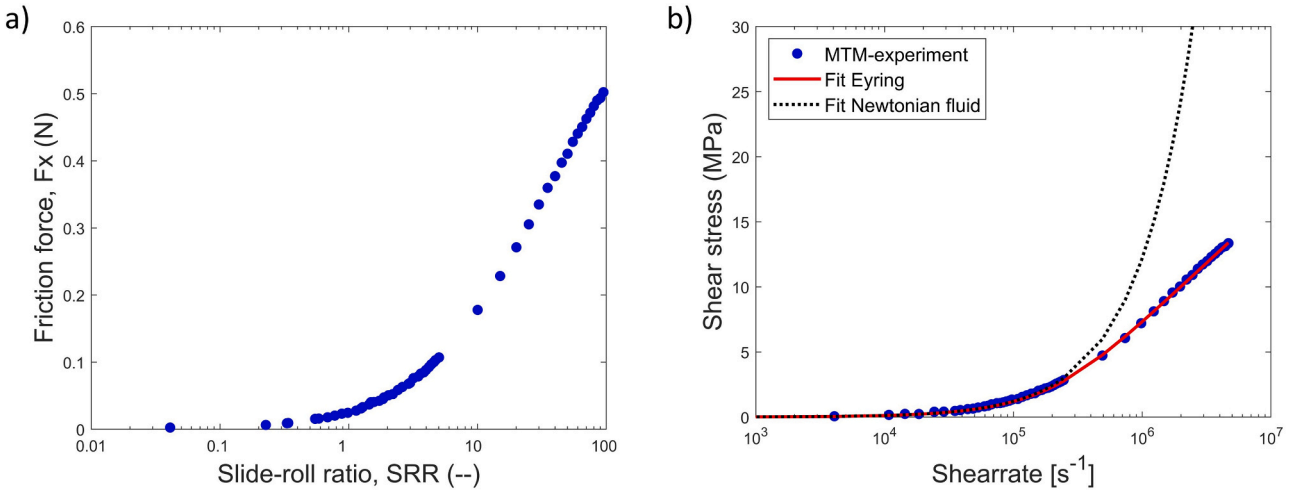

Fig. 6. a) typical result of an MTM-experiment (for a load of 20 N at a temperature of 40°C), friction force F_x as a function of slide-roll-ratio *SRR*; b) MTM-results expressed as shear stress vs. shear rate, the best fit for a Newtonian fluid (Eq. (6)) and the best fit with the Eyring equation (Eq. (7)).

for all experiments, i.e. all combinations of lubricant pressure and temperature. The obtained parameters are plotted as function of pressure and temperature in Figs. 7 and 8, together with the best fit of the corresponding rheological relation which will be used for the analysis of the other experiments.

In Fig. 7, the best fit of the measurement results with the extended Roelands equation is shown. There is good agreement between measurements and fit, except for the experiments at low pressure and high temperature (which is quite an uncommon combination in industrial cold rolling). The parameters of this best fit are given in Table 5.

Fig. 8 shows that the limiting Newtonian shear stress τ_0 increases with lubricant pressure, however the influence of lubricant temperature is not clear. The following fit function, also shown in Fig. 8, will be used to validate the hydrodynamic rolling trials at the pilot mill:

$$\tau_0 = 0.0061 \cdot p_{\text{lub}} + 0.4 MPa \tag{14}$$

Such a linear relation between the limiting Newtonian shear stress and pressure was also measured on a two-disk machine by Evans [56] for some of his lubricants.

These results now fully characterise the viscosity and viscous shear stress of the RK1832DR lubricant as a function of pressure and temperature. In Sections 4.2 to 4.4, this characterisation will be used to validate both film thickness measurements on the EHL-rig, as well as film thickness measurements and cold rolling experiments on the pilot mill.

In this section another result of the MTM-experiments is shown. To determine the relevance of viscous shear in cold rolling, compared to other friction mechanisms (such as adhesive friction and ploughing friction), the coefficient of friction (COF) resulting from viscous shear in the MTM-experiments is plotted as function of temperature and pressure in Fig. 9.

From Fig. 9 it can be concluded that:

- Only for a combination of low temperature (40°C) and high pressure the thermal regime is reached. The data points in the thermal regime are not considered when determining $\eta(p,T)$ and $\tau_0(p,T)$ via the procedure detailed in Section 2.
- For many combinations of temperature, pressure and shear rate that are common in cold rolling of steel, the viscous COF is of the same order of magnitude as the total COF in the cold roll bite (which ranges typically between 0.015 and 0.06 according to Yuen et al. [57]). It must be concluded that the contribution of viscous shear stress to the overall COF cannot be neglected.

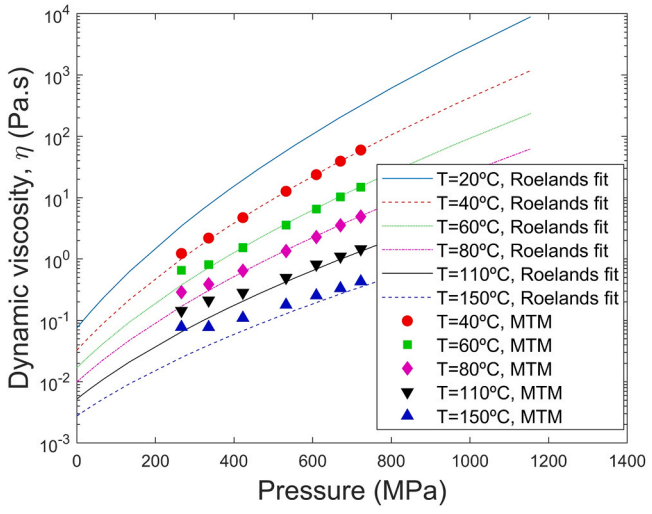

Fig. 7. markers: MTM-results of viscosity as function of temperature and pressure, lines: Roelands equation that fits best with measurement results. The Roelands parameters are given in Table 5.

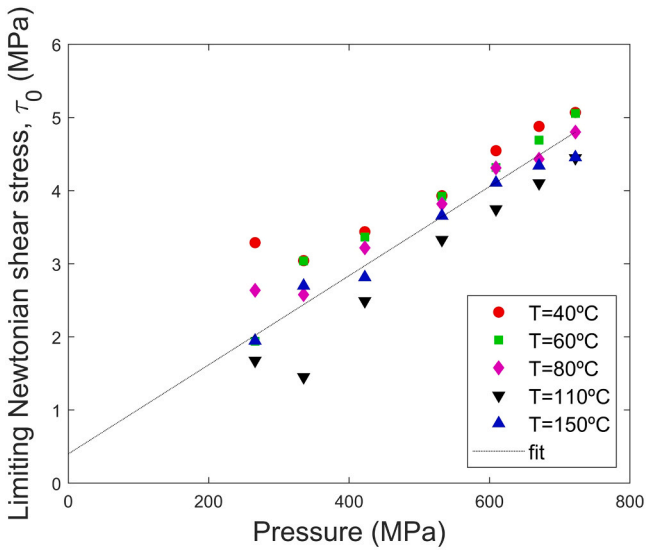

Fig. 8. limiting Newtonian shear stress values, determined with the MTM-experiments, as a function of lubricant pressure and temperature. The line represents the fit that is used in the cold rolling model.

Table 5
parameters in Roelands equation, resulting in best agreement with MTM-results.

Roelands parameters	Value deduced from MTM-experiments
$\eta_{p_{atm},T_{ref}}$ [Pa·s][a]	0.03245 (at 40°C)
s_0 [–][a]	1.031
C_{ROE} [–]	-0.04825
D_{ROE} [–]	0.4990

[a] *$\eta_{p_{atm},T_{ref}}$ and s_0 were determined by the standard viscometer at ambient pressure and temperatures between 20 and 80°C.*

- Viscous shear stresses vary significantly in the roll bite: around the neutral point the shear rate is low and viscous shear stresses can be neglected, at the roll bite entry the shear rate can easily be as high as 10^7 s^{-1} and viscous stresses are significant, even up to very high temperature.

4.2. EHL-rig

Disk speed and ball speed are kept equal during the EHL-experiments. In Fig. 10 the measured lubricant film thickness is plotted against this process speed for various lubricant temperatures. The pressure-viscosity coefficient $\alpha^*(T)$ can be determined with the Roelands parameters in Table 5 and Eqs. (5) and (10), enabling the determination of the predicted film thickness based on Moes [23] formula (Eq. (A.7)), which is also shown in Fig. 10.

As shown in Fig. 10, especially at low process speed the measurements correspond fairly well with the modelled film thickness. At higher process speed, the measured film thickness is lower than the predicted value which is probably related to heat generation due to high shear rate in the lubricant film, this is not taken into account in the Moes equation. The average error in the film thickness prediction is 20%, Moes [23] mentions that the accuracy of his formula is within 10%, especially at higher speed the differences between model and measurement are slightly higher.

Overall, it can be concluded that the viscosity as determined by the MTM-experiments allows to predict the film thickness in the EHL-experiments reasonably well. It can be concluded that the presented method, to derive lubricant properties from the MTM-experiments, is feasible.

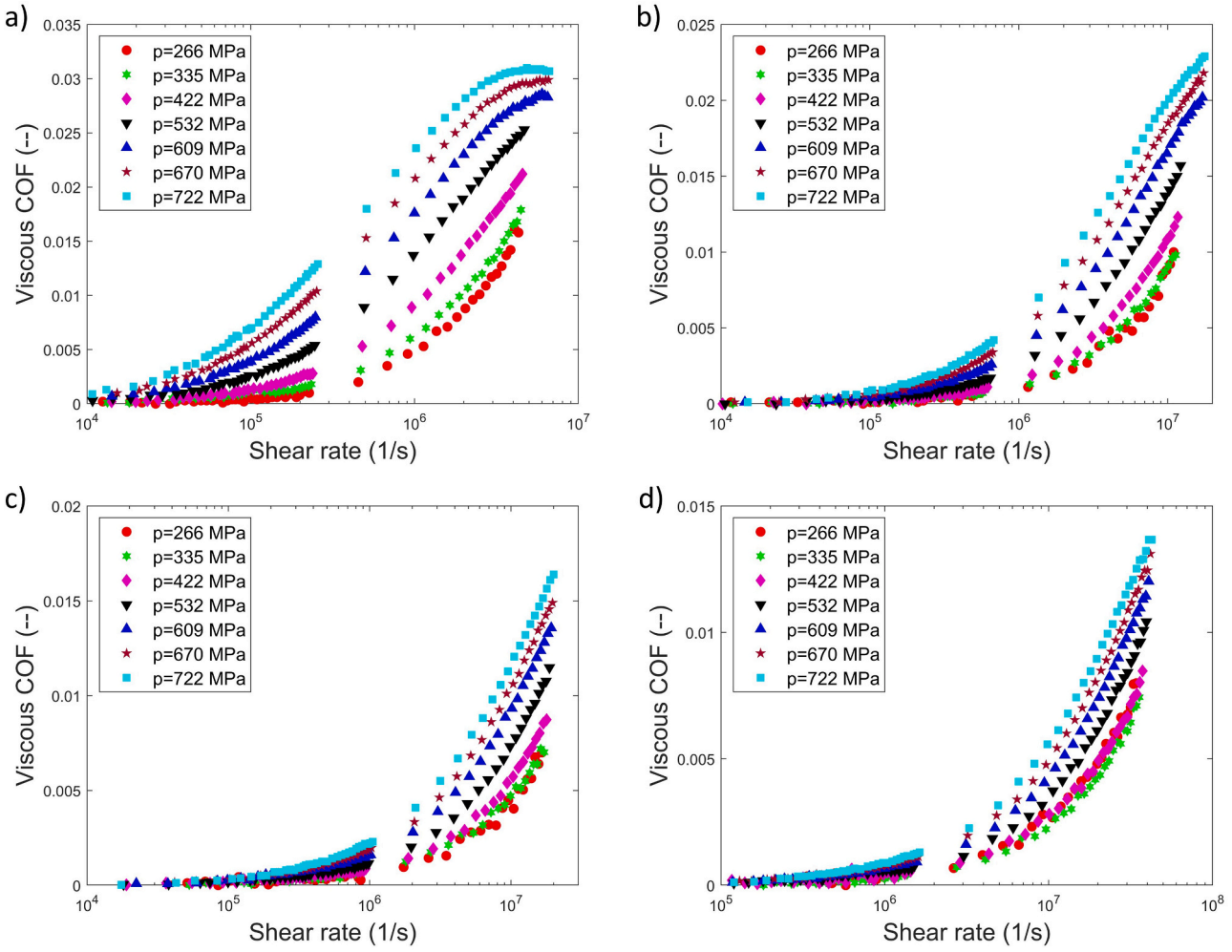

Fig. 9. viscous coefficient of friction (COF) as function of pressure, speed and lubricant temperature; a) 40 °C, b) 80 °C, c) 110 °C, d) 150 °C.

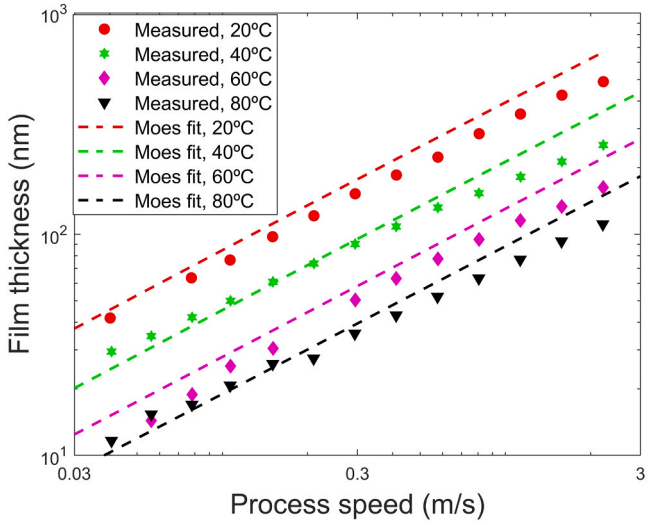

Fig. 10. film thickness measurements on EHL-rig as function of process speed and comparison with Moes formula (Eq. (A.7)). The markers indicate the measurements, the lines indicate the results from the Moes equation.

4.3. Droplet trials

Jacobs et al. [55] showed that without any correcting measures, the strip material is likely to enter the roll bite asymmetrically which has a significant influence on the measured lubricant film thickness. This insight was obtained during the currently described research, therefore in this work also droplet trials were carried out with asymmetric feeding (in test 1,2 and 3) while symmetric strip feeding was applied only in the third test. Jacobs et al. [55] compared droplet trials with symmetric and asymmetric strip feeding to establish a correction factor. This correction factor, that only seems to depend on the strip thickness, is then used to 'correct' the droplet trials that were carried out under asymmetric feeding conditions, it is given by:

$$\begin{aligned} C(t_{in}) &= \frac{h_{\mathrm{lub},sym}}{h_{\mathrm{lub},asym}} = -0.4946 \cdot t_{in} + 1.2635 \quad 0.53mm < t_{in} < 1.6mm \\ C(t_{in}) &= 1 \qquad\qquad\qquad\qquad\qquad\qquad\quad t_{in} < 0.53mm \end{aligned} \tag{15}$$

Where $h_{\mathrm{lub},sym}$ and $h_{\mathrm{lub},asym}$ are the measured lubricant film thickness at the roll bite exit if the strip is fed symmetrically resp. asymmetrically to the roll bite. With the model described in Section 2.2 (and Eq. (11)), the film thickness for each droplet experiment was determined. Obviously, the model used again the viscosity-pressure-temperature relation obtained from the MTM-experiments, as summarised in Table 5. The comparison between model and measurement is shown in Fig. 11. For transparency, a different marker is used for each test and to indicate uncorrected results for processes with symmetric strip feeding and

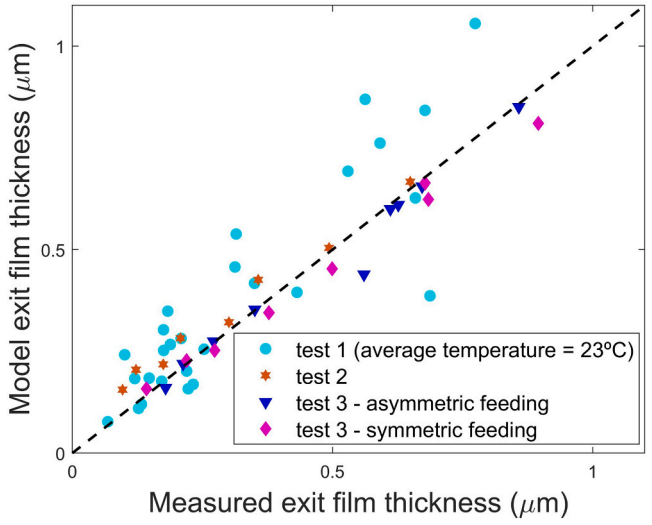

Fig. 11. measured lubricant film thickness at the exit of the roll bite as function of the modelled lubricant film thickness.

corrected results for processes with asymmetric strip feeding.

Fig. 11 shows a good agreement between theoretical and experimental results, the average error in the lubricant film thickness prediction is 0.07 μm (for droplet test 2 and 3, in which the strip and roll temperatures were recorded, the average error is only 0.03 μm). This shows that the lubricant film thickness in cold rolling can be predicted accurately enough when an accurate viscosity-pressure-temperature relation is used.

4.4. Hydrodynamic lubrication trials

The model used in the previous section to calculate lubricant film thickness for the droplet trials, is also used in this section to determine the lubricant film thickness for the hydrodynamic lubrication trials. The results of these calculations are given in Table 6 together with the combined strip and work roll roughness and the λ-parameter which is indicative of the lubrication regime ($\lambda = h_{entry}/R_{q,comb}$) while the combined roughness is calculated with [8]:

$$R_{q,comb} = \sqrt{R_{q,strip}^2 + R_{q,roll}^2} \tag{16}$$

With $R_{q,roll}$ and $R_{q,strip}$ the R_q-values of the surface topography of strip and roll. For $\lambda > 3$ the lubrication regime is hydrodynamic (see for example Boemer [8]); for the first test this is achieved because of the small thickness reduction and low strip/roll roughness. In the second test the lubrication regime is almost hydrodynamic, but some contact between work roll and strip asperities can be expected.

For each rolling experiment, the measured rolling force and forward slip are averaged over time. The forward slip is defined as $s_f = (v_{strip,exit}/v_{roll} - 1)\cdot 100\%$, low rolling force and low forward slip are both indicative of a well lubricated contact. A comparison between the measured and modelled rolling force and forward slip is given in Fig. 12.

Table 6
calculated film thickness, measured $R_{q,comb}$ and derived λ-value for each hydrodynamic rolling trial.

Test nr	h_{entry} (μm)	$R_{q,comb}$ (μm)	λ (–)
1A	1.7	0.7	2.5
1B	1.5	0.5	3.1
1 C	1.6	0.5	3.0
1D	1.7	0.5	3.8
2A	1.5	0.8	1.4
2B	1.5	1.0	1.2
2 C	1.8	1.0	1.4
2D	2.0	1.0	1.6
2E	1.8	1.0	1.4

Fig. 12 shows that not only the model converges for each rolling process, but it also gives a fairly good prediction, both of rolling force and forward slip. The average difference between predicted and measured forward slip is 1% point, while the accuracy of the calculated rolling force is 10% of the measured force. This indicates that the (viscous) shear stresses are more or less correctly taken into account in the model. It should be reminded here that this rolling model does not contain a coefficient of friction anymore, hence there is no "fit-parameter" in the model. Normally cold rolling models rely heavily on such a coefficient to match modelled results with experiments. This model is purely based on theoretical relations and measured material properties such as the stress-strain curve in Fig. 5 and the viscosity from the MTM-experiments.

Because of elastic recovery, the strip speed slightly decreases at the roll bite exit. As shown in Fig. 12, this can result in the model predicting a small negative forward slip. The measured slip can become much more negative. The rolling model could be extended with the possibility to predict such high negative forward slip (similar as [58]), but in this version of the model, because of the chosen method of iteration, it is not possible.

For the last process, experiment 2E, the evolution of the coefficient of friction due to viscous shear stress over the contact length as well as the resulting friction hill is given in Fig. 13.

According to Fig. 13, in these hydrodynamic lubrication experiments the friction hill is much less pronounced than usual for a cold rolling process. This is due to the low friction and the high exit tension (compared to entry tension) which is necessary to avoid skidding of the work rolls. Furthermore, Fig. 13 clearly shows that for a large part of the roll bite, the viscous shear stresses are not negligible, as was already shown in Fig. 9.

5. Discussion

In the previous section it was shown that the viscosity-pressure-temperature relation, as derived from MTM-experiments, enabled a good prediction of film thickness and viscous shear, both on the EHL-rig and on the pilot mill. This resulted in a cold rolling model without any fit parameters, that gives good prediction of forward slip and rolling force in a hydrodynamic cold rolling process. The experimental results are further discussed in this section.

5.1. Measured viscosity-pressure-temperature relation

The results presented in Fig. 7 show that the MTM-results can be accurately described by the Roelands equation. Only for the combination of high temperature and low pressure, the measured viscosity is significantly higher than the best fit with the Roelands equation. It cannot be excluded that this is related to the experiment because for these conditions the lubricant film thickness becomes so small that elastohydrodynamic lubrication is not guaranteed anymore. For a lubricant temperature of 150ºC, the lubricant film thickness according to the Moes-formula is only between 30 and 40 nm. Although no signs of wear were observed, there may have been incidental contact between the ball and disk in the MTM-experiments. Furthermore, as remarked by Liu et al. [59], at low pressure the contact region is underestimated by Hertzian theory (while at high pressure the Hertzian approximation is valid [59]). In any case, the combination of low pressure and high temperature is unlikely to exist in a cold rolling mill for low Carbon steel, therefore the discrepancy between the measurements and the Roelands equation is of little practical importance for the cold rolling industry.

An often-made assumption is that the Barus formula (Eq. (2)) can be used to describe the lubricant viscosity at high pressure. To investigate this assumption, the viscosity according to the Roelands equation is

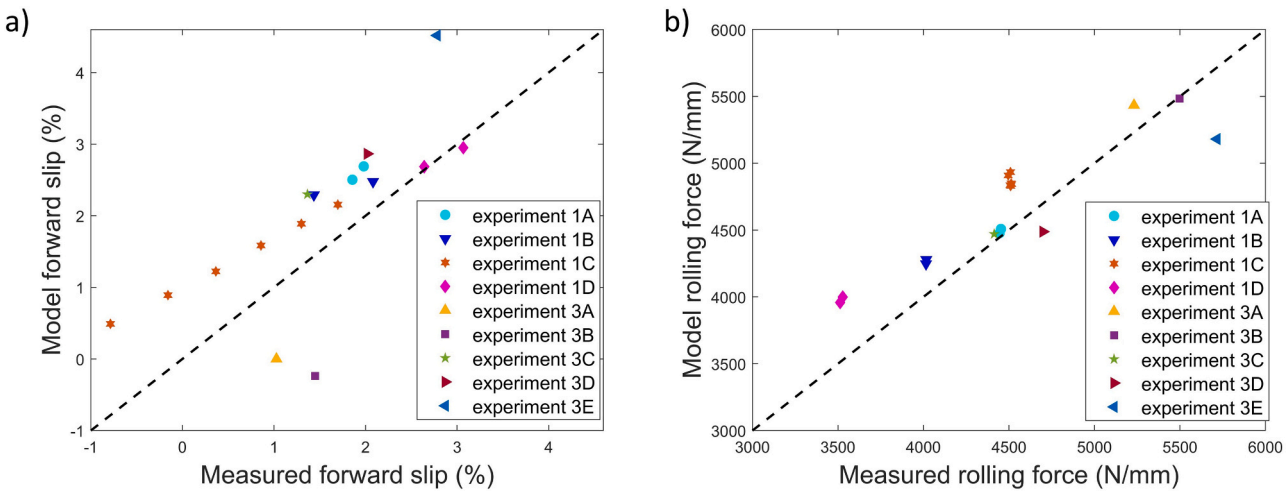

Fig. 12. comparison of model simulations with experimental results of the hydrodynamic lubrication experiments; a) forward slip, b) rolling force.

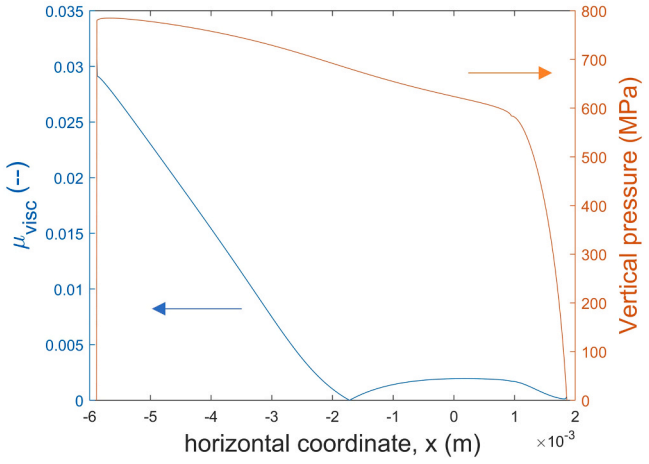

Fig. 13. modelled distribution of vertical pressure and shear stress divided by vertical pressure in the roll bite (for test 2E at 10 m/s).

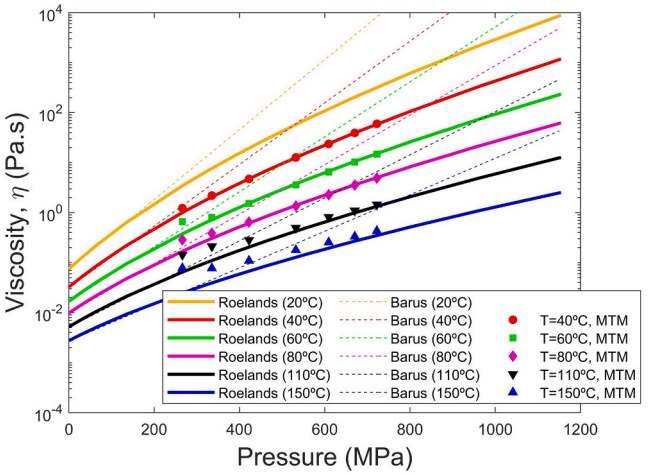

Fig. 14. Comparison of viscosity according to Roelands equation (best fit with MTM-results) as well as viscosity according to Barus based on equivalent pressure-viscosity coefficient α^* (from Eq. 9).

compared with Barus-equation in Fig. 14. The results with the Barus equation are based on the equivalent pressure-viscosity coefficient α^* as defined in Eq. (9). Fig. 14 shows that, depending on lubricant temperature, the Barus equation rather accurately predicts the viscosity up to a pressure of 200–400 MPa. At higher pressure the Barus-equation overestimates the viscosity as determined in the MTM-experiments.

It can be concluded that for the rolling of softer metals, where the average rolling pressure does not exceed a few hundreds MPa, the Barus equation gives an accurate description of the pressure-viscosity relation. For the rolling of low Carbon steel, where the pressure can easily be as high as 1 GPa, the Barus equation significantly overestimates the lubricant viscosity at high pressure and the Roelands equation should be preferred. Obviously, these conclusions are based on the measurement results for the RK1832DR oil, for another lubricant the conclusions could be different.

It is interesting to discuss how the results of Fig. 14 relate to a direct measurement of viscosity at high pressure. In his measurements, Bair finds that for all glass-forming lubricants the η, p-graph shows an inflection point, from slower to faster than an exponential law [21]. It is stated that this inflection occurs at a material-specific viscosity [25] and it can be inferred that it occurs at a pressure of approximately 1 GPa. As the pressures in Fig. 14 are lower than 1 GPa, these can also be described by the Roelands law that clearly captures only the part where the viscosity increase is slower than exponential. Nevertheless, it cannot be excluded that a small error in the prediction of viscosity (by the Roelands equation) is offset by a small error in the coefficients for the Eyring equation.

5.2. *Discussion of experimental results*

The relatively small deviations between experimental results (on EHL-rig and pilot mill) and theory could well be related to the temperature control during the experiments. As shown in Fig. 7, a small deviation in lubricant temperature leads to a relatively large change in viscosity and hence in measured lubricant film thickness or viscous shear stress. Although it is not straightforward, in the MTM and EHL-experiments provisions are foreseen to control the temperature. However, in the rolling experiments the temperature cannot be controlled as a significant amount of energy is dissipated because of plastic deformation and friction. In the droplet experiments, the temperature in the inlet zone is most relevant so the influence of plastic deformation is only limited. However, in the hydrodynamic rolling experiments it is relevant how the lubricant temperature evolves in the roll bite. Therefore, assumptions need to be made; Boemer [8] gives different thermal scenarios for the lubricant in the roll bite:

- Isothermal: the lubricant temperature remains equal to its application temperature.
- The lubricant temperature is equal to its application temperature, but if the strip temperature is higher the lubricant takes over the strip temperature.
- The lubricant temperature increases due to frictional heat generated in the lubricant.

Another likely scenario is that the lubricant temperature is the average of work roll and strip temperature. To decide between these different possibilities, it is insightful to determine the thermal penetration depth of the lubricant. According to Faghri and Zhang [60], for a semi-infinite body this depth is given by:

$$\delta_{TH} = \sqrt{8 \cdot D \cdot t} \tag{17}$$

Where D is the thermal diffusivity and t is the contact time. The thermal diffusivity of a paraffin oil (at room temperature) is approximately 0.08 mm^2/s [61]. In an actual rolling process, a typical contact time of the sheet and the roll is in the order of 1 millisecond. This corresponds with a penetration depth of 25 μm, much larger than the lubricant film thickness. It is therefore reasonable to assume that the lubricant temperature is regulated by the temperature of the work roll and the strip. The validity of this method is further confirmed by experiments of Liu et al. [62], who show that the initial lubricant temperature has relatively little influence on elastohydrodynamic lubricant film build up, however the temperature of the disk has great influence on the lubricant film build up.

In experiment 1 C the entry tension was changed in 6 steps, which had a marked influence on the measured forward slip. Fig. 12 shows that the influence of entry tension on forward slip is not perfectly predicted by the model. Fig. 15 shows model results for experiment 1 C but with a lubricant temperature that is 10 °C higher than in Fig. 12, this figure shows how sensitive the forward slip (and hence friction) is for a relatively small change in temperature, for clarity the results are plotted against the measured slip values as in Fig. 12.

For a rolling process in the mixed lubrication regime, the influence of temperature on forward slip should be less. An increase in temperature still leads to a smaller contribution of viscous shear, but this is offset by a larger true contact ratio because also the film formation will be lower. Therefore in industrial cold rolling, the influence of a small error in the temperature prediction should be less than the results shown in Fig. 15.

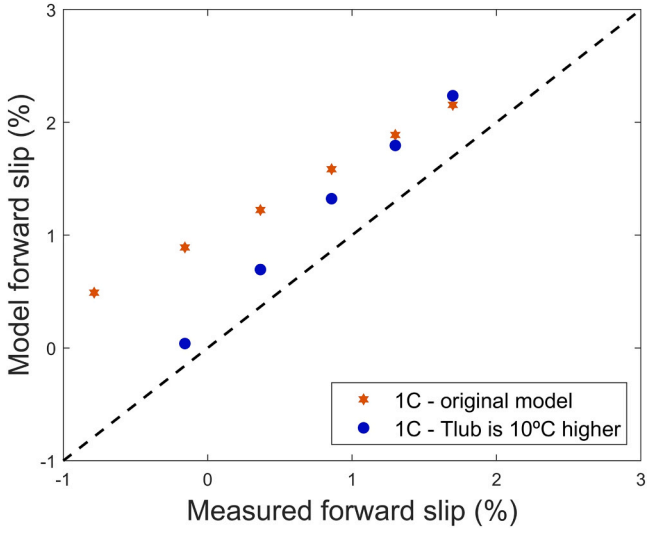

Fig. 15. influence, according to the rolling model, of a relatively small change in lubricant temperature on the prediction of forward slip for experiment 1 C.

5.3. Relevance of viscous shear in industrial cold rolling

The relevance of this work for industrial cold rolling mills, that operate in the mixed lubrication regime, should be discussed. Most generally it can be stated that in the mixed lubrication regime the asperities carry a part of the rolling load and the friction in the roll bite can be calculated with the equivalent of the load sharing relation [63]:

$$\tau(x) = A\tau_{asp} + (1-A)\tau_{visc} = A\tau_{asp} + (1-A)\tau_0(p,T)\cdot \mathrm{asinh}\left(\frac{\eta(p,T)\cdot\dot{\gamma}}{\tau_0(p,T)}\right) \tag{18}$$

In this equation A is the true contact ratio, τ_{asp} is the average shear stress at the asperity contacts and τ_{visc} is the viscous shear stress given by Eq. (7). The term $(1-A)\tau_{visc}$ is the contribution of viscous shear stress in a mixed lubricated rolling contact.

As in the Mixed Lubrication regime $A > 0$, at first sight it appears that the contribution of viscous shear stress is lower than in a purely hydrodynamic contact. However, the shear rate in the lubricant, $\dot{\gamma}$, is higher because the lubricant film thickness is lower. Wilson and Chang [64] showed that the lubricant pressure increases very quickly after the plastic deformation starts, in what they call the 'transition zone'. According to this accepted theory, even at very low rolling speed, the lubricant film becomes fully pressurized and hence hydrodynamic effects play a role. As a consequence, the available lubricant in the rolling contact will always be pressurized up to a pressure equal to the average pressure in the contact. Therefore in the biggest part of the strip/roll-contact, both $\tau_0(p,T)$ and $\eta(p,T)$ in Eq. (18) do not substantially depend on the lubrication regime.

The relation between true contact ratio and average lubricant film thickness is determined by the surface topographies of roll and strip surface. A normally distributed surface topography can be approximated by a Christensen topography, with the following height distribution function [65]:

$$f(h) = \frac{35}{96R_{q,comb}}\left(1-\left(\frac{h}{3R_{q,comb}}\right)^2\right)^3 \qquad -3R_{q,comb} < h < 3R_{q,comb} \tag{19}$$

Where h is the height of the combined roughness. This equation can be used to determine the relation between true contact ratio and average lubricant film thickness which is shown in Fig. 16a. With this relation it is then possible to determine the contribution of viscous shear in a mixed lubrication contact. This exercise has been carried out for the process of trial 2E. Fig. 16b shows the contribution of viscous shear stress in a mixed lubricated rolling contact with true contact ratios fixed at 0.25, 0.5 and 0.75. For easy comparison, the values are divided by the vertical pressure so that, analogous to Fig. 13, a viscous coefficient of friction is obtained.

In a cold rolling process the true contact ratio is not constant but increases towards the roll bite exit. Fig. 16b shows that up to fairly high true contact ratios, the contribution of viscous shear stress (to the total friction) cannot be neglected as it is in the same order of magnitude as the total COF in the cold roll bite. It should be mentioned that in reality a sticking zone exists, especially when the thickness reduction is small [66]. Obviously there is no contribution of viscous shear stress in such a sticking zone. The sticking zone is positioned around the location where the classical rolling model finds a neutral point and therefore low viscous shear stress. Therefore the influence of a sticking zone on the distribution of viscous shear stress is only limited.

The presented rolling model assumes that the shear in the lubricant is low enough so that the thermal regime is not reached. In the thermal regime so much heat is developed in the lubricant film that the viscosity decreases considerably with a further increase in shear rate. As a consequence also the viscous shear stress (and the lubricant film thickness) will decrease. In the presented MTM-experiments, the thermal regime was only observed at a lubricant temperature of 40ºC. The results presented in Fig. 9 suggest that the thermal regime starts when $\mu_{visc} \approx 0.03$, but measurement at even higher shear rates would be

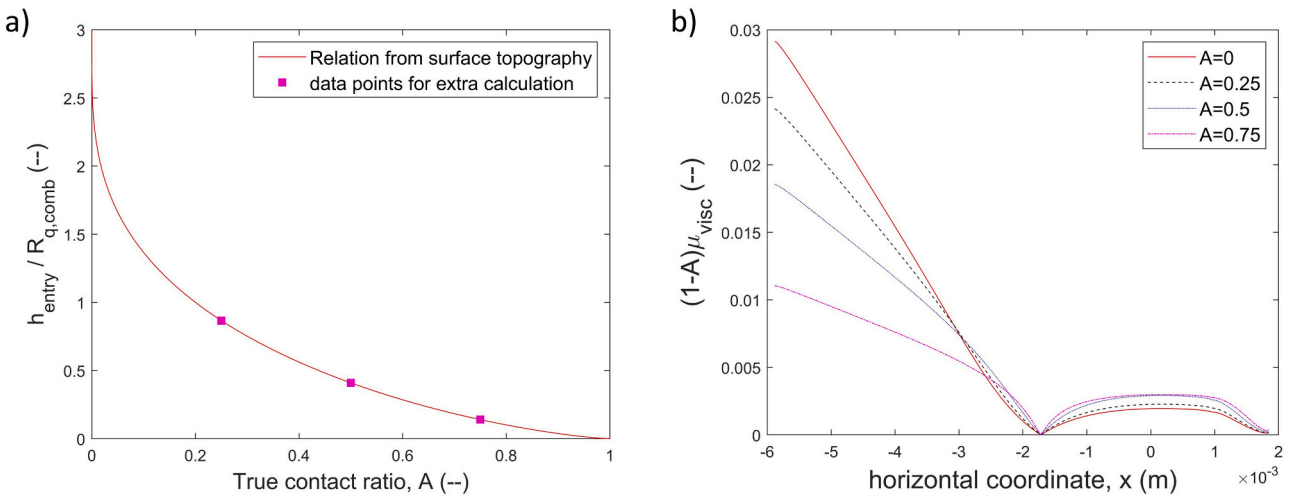

Fig. 16. a) relation between true contact ratio *A* and normalised film thickness for a Christensen surface topography, b) calculated contribution of the viscous shear to the overall coefficient of friction in a mixed lubricated cold rolling contact. For the calculation the data of experiment 2E were used.

necessary to determine when the thermal regime starts at higher lubricant temperatures. In an industrial mill it is therefore not so likely that the thermal regime will be reached, but it cannot be totally excluded either. More experimental effort would be needed to integrate this possibility in the cold rolling model.

6. Conclusions

Usually viscous shear stress is neglected in Mixed-Lubrication cold rolling models for low-carbon steel. This work investigates the relevance of viscous shear as a friction mechanism in a mixed lubricated cold rolling contact. Experiments have been carried out, both on laboratory equipment and a semi-industrial pilot mill. The following conclusions can be drawn from the work presented in this article:

- The presented work shows that in a typical industrial cold rolling process, the viscous shear stress substantially contributes to the total coefficient of friction.
- At pressures, temperatures and shear rates that are common in cold rolling of low Carbon steel, the investigated lubricant shows non-Newtonian behaviour. The observed behavior can be described with the Eyring equation (Eq. (7)) for viscous shear stress.
- It is not sufficient to use the commonly used Barus-equation (Eq. (2)) to model the cold rolling process of low-carbon steel. The rheological behaviour of the investigated lubricant can better be described with the extended Roelands equation (Eqs. (4) and (5)).
- Both the viscosity-pressure-temperature relation as well as the shear behavior of a cold rolling lubricant can be accurately characterised with MTM-experiments.
- The measured rheological relations are integrated in a cold rolling model. The developed model is purely based on measured properties of strip, work roll and lubricant, no (unknown) friction factor is necessary anymore. For hydrodynamic rolling, the model predicts the forward slip with an average deviation of 1% point from the measured values, while the accuracy of the calculated rolling force is 10% of the measured force.

CRediT authorship contribution statement

L.J.M. Jacobs: Writing – original draft, Conceptualisation, Methodology, Investigation, Validation. **J. van der Lugt**: Supervision, Project administration, Writing – review & editing. **M.B. de Rooij**: Conceptualisation, Supervision, Project administration, Writing – review & editing.

Declaration of Competing Interest

The authors declare that they have no known competing financial interests or personal relationships that could have appeared to influence the work reported in this paper.

Data availability

Data will be made available on request.

Acknowledgement

The authors kindly thank Tata Steel and TotalEnergies for permission to publish this document. Furthermore they like to thank Daphne van de Giesen, Hans Weel and Brian du Pont for their help in setting up the pilot mill experiments and carrying out the trials.

Appendix A. , Moes-formula

The Moes equation was developed to describe the film thickness in the EHD-regime, it is based on the theoretical asymptotic solution of the central film thickness in 4 cases (i.e. H_{RI} for the rigid isoviscous case, H_{EI} for the elastic isoviscous case, H_{RP} for the rigid piezoviscous case and H_{EP} for the elastic piezoviscous case). The 'asymptotic' solutions for these cases are all expressed in 2 parameters N_{Moes} and L_{Moes}, that summarize the process and lubrication conditions. N_{Moes} and L_{Moes} are defined as:

$$N_{Moes} = \sqrt{\frac{R_x}{R_y}}\frac{F}{E' \cdot R_x^2}\left(\frac{E' \cdot R_x}{\eta_{p_{atm},T_{ref}} \cdot U}\right)^{0.75} \tag{A.1}$$

$$L_{Moes} = \alpha^* E^{'} \left(\frac{\eta_{p_{atm},T_{ref}} \cdot U}{E^{'} \cdot R_x} \right)^{0.25} \tag{A.2}$$

Here R_x and R_y are the equivalent radii of curvature in x,y-direction, which are obviously equal in the MTM-experiments. Furthermore F is the load on the ball and U is the sumspeed of disk and ball. The asymptotic solutions (for $\frac{R_x}{R_y} = 1$) are then given by:

$$H_{RI} = 145 \cdot (1.796)^{-15/7} \cdot N_{Moes}^{-2} \tag{A.3}$$

$$H_{EI} = 3.18 \cdot (1.63)^{-14/25} \cdot N_{Moes}^{-2/15} \tag{A.4}$$

$$H_{RP} = 1.29 \cdot (1.691)^{-2/3} \cdot L_{Moes}^{2/3} \tag{A.5}$$

$$H_{EP} = 1.48 \cdot (1.63)^{-7/20} \cdot N_{Moes}^{-1/12} \cdot L_{Moes}^{3/4} \tag{A.6}$$

The central film thickness can then finally be calculated with the following fit, which is necessary to provide a smooth transition between the asymptotic solutions:

$$h_c = R_x \left(\frac{E^{'} \cdot R_x}{\eta_{p_{atm},T_{ref}} \cdot U} \right)^{-0.5} \cdot H_{Moes} \tag{A.7}$$

Where H consists of the fit function with the different asymptotic solutions:

$$H_{Moes} = \left\{ H_{RI}^{2/3} + \left(H_{EI}^{-4} + 0.1 \right)^{-3/8} \right\}^{2s/3} + \left(H_{RP}^{-8} + H_{EP}^{-8} \right)^{-s/8} \tag{A.8}$$

And s defined as:

$$s = \left\{ H_{RI}^{2/3} + \left(H_{EI}^{-4} + 0.1 \right)^{-3/8} \right\}^{2s/3} + \left(H_{RP}^{-8} + H_{EP}^{-8} \right)^{-s/8} \tag{A.9}$$

For the settings in the MTM-experiments, Moes 2000 reports that this fit corresponds within 10% to numerical calculations.

The minimum film thickness is approximately ¾ of the central film thickness, but as the minimum film thickness occurs only very locally, it is common to use the central film thickness to analyse the MTM and EHL experiments.

The iterative procedure to determine the rheological parameters τ_0 and z from the MTM-experiments is visualised in Figure A1. For a given value of z, the viscosity can be determined with the Roelands equation.

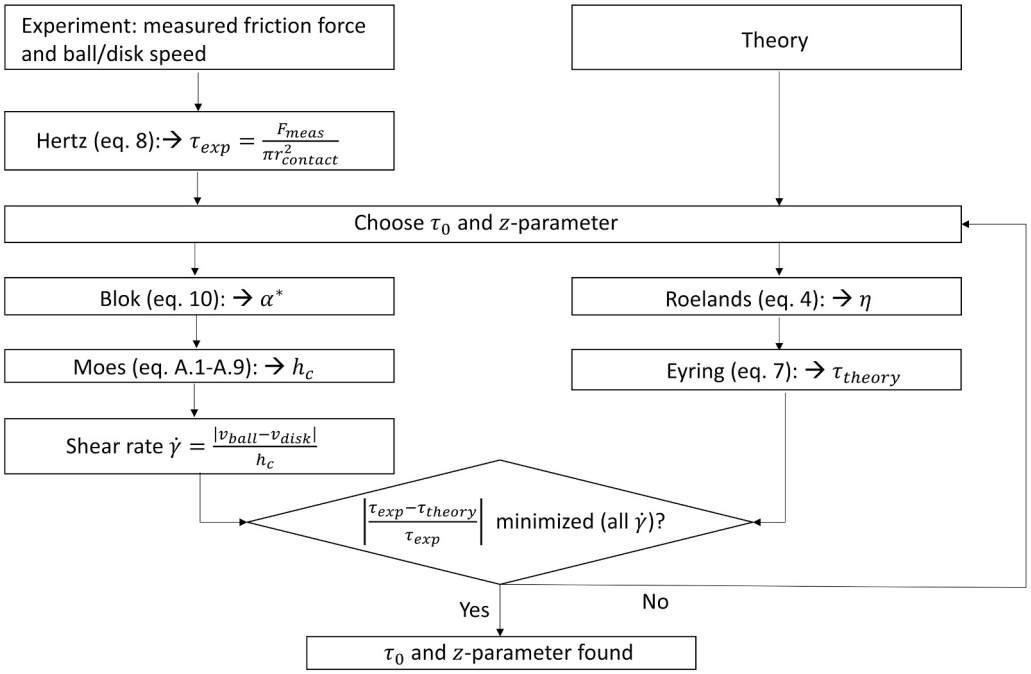

Fig. A1. schematic presentation of the iterative procedure to determine the rheological parameters τ_0 and z from the MTM-experiments.

.

References

[1] Roberts CD. Mechanical principles of rolling. Iron Steelmak 1997;vol. 24:123–4.
[2] Heidari A, Forouzan MR, Niroomand MR. Development and evaluation of friction models for chatter simulation in cold strip rolling. Int J Adv Manuf Technol 2018; vol. 96:2055–75. https://doi.org/10.1007/s00170-018-1658-x.
[3] Lu X, Sun J, Wei Z, Li G, Zhang D. Effect of minimum friction coefficient on vibration stability in cold rolling mill. Tribology Int 2021;vol. 159:106958. https://doi.org/10.1016/j.triboint.2021.106958.
[4] Mekicha MA, de Rooij MB, Matthews DTA, Pelletier C, Jacobs L, Schipper DJ. The effect of hard chrome plating on iron fines formation. Tribology Int 2020;vol. 142: 106003. https://doi.org/10.1016/j.triboint.2019.106003.
[5] Montmitonnet P, Bouadjadja N, Luong LP, Bertrandie JJ, Dietsch H. On the mechanism by which chromium improves strip surface cleanliness in steel strip cold rolling. Key Eng Mater 2018;vol. 767:240–7. https://doi.org/10.4028/www.scientific.net/KEM.767.240.
[6] Shimura M, Kasai D, Shiraishi T, Takahama Y. Fundamental study of lubrication characteristics of high strength steel in cold rolling. Proc Int Roll Conf, Sao Paulo 2019. https://doi.org/10.5151/9785-9785-32189.
[7] Wu C, Zhang L, Qu P, Li S, Jiang Z. HD-lubricated High-speed Small Reduction Rolling of Hard Steel Strip with Elastically Deformable Rolls. Tribology Int 2022; vol. 165:107295. https://doi.org/10.1016/j.triboint.2021.107295.
[8] Boemer D. Numerical Modeling of Friction in Lubricated Cold Rolling (PhD-thesis). University of Liege,; 2020 (PhD-thesis), ⟨http://hdl.handle.net/2268/245441⟩.
[9] Smeulders JBAF. Novel laboratory lubrication tests for cold rolling emulsions. IronSteel Technol 2015;vol. 12:56–64.
[10] Bergmann M., Krimpelstatter K., Nilsson B., Karakavaf S. and Leffers R. 2019. Intelligent Roll-gap Lubrication Improves Strip Surface Cleanliness in Thyssenkrupp Steel's Tandem Cold Rolling Mill, *ESTAD conference Dusseldorf*.
[11] Laugier M, Tornicelli M, Leligois CS, Bouquegneau D, Launet D, Alvarez JA. Flexible lubrication concept. The future of cold rolling lubrication. Proc Inst Mech Eng, Part J: J Eng Tribology 2011;Vol. 225:949–58. https://doi.org/10.1177/1350650111414514.
[12] Bhushan B. Introduction to tribology. John Wiley & Sons,; 2013. *ISBN 978-1-119-94453-9*.
[13] Von Karman T. Beitrag zur Theorie des Walzvorganges. Z für Angew Math und Mech 1925;5:139–41. https://doi.org/10.1002/zamm.19250050213.
[14] Roberts WL. Cold Rolling of Steel. *New York and Basel*: Marcel Dekker Inc,; 1978.
[15] Nadai A. The forces required for rolling steel strip under tension. J Appl Mech 1939;vol. 6:54–62. https://doi.org/10.1115/1.4008920.
[16] Wilson WRD, Walowit JA. An isothermal hydrodynamic lubrication theory for strip rolling with front and back tension. Tribology Conv, Inst Mech Eng, Lond 1971;93: 164–72.
[17] Lugt P. Lubrication in Cold Rolling – Numerical Simulation using Multigrid Techniques (PhD-thesis). University of Twente,; 1992.
[18] Marsault N. 1998. Modélisation du régime de lubrification mixte en laminage à froid, *PhD-thesis école des Mines*.
[19] Azushima A. Characteristics of lubrication in cold sheet rolling. *Proceedings 1st International Conference on Lubrication Challenges in Metalworking and Processing*. ITT Research Institute Chicago,; 1978. p. *81–7*.
[20] Azushima A. Tribology in Sheet Rolling Technology. Springer International Publishing AG Switzerland,; 2016. https://doi.org/10.1007/978-3-319-17226-2.
[21] Bair S, Martinie L, Vergne P. Classical EHL Versus Quantitative EHL: A Perspective Part II — Super-Arrhenius Piezoviscosity, an Essential Component of Elastohydrodynamic Friction Missing from Classical EHL. Tribology Lett 2016;vol. 63:37. https://doi.org/10.1007/s11249-016-0725-4.
[22] Bair S. The rheological assumptions of classical EHL: What went wrong? Tribology Int 2019;vol. 131:45–50. https://doi.org/10.1016/j.triboint.2018.10.020.
[23] Moes H. Lubrication and Beyond. Lecture notes code 115531. University of Twente,; 2000.
[24] Spikes H, Jie Z. History, origins and prediction of elastohydrodynamic friction. Tribology Lett 2014;vol. 56:1–25. https://doi.org/10.1007/s11249-014-0396-y.
[25] Bair S, Vergne P, Kumar P, Poll G, Krupka I, Hartl M, Habchi W, Larsson R. Comment on 'History, Origins and Prediction of Elastohydrodynamic Friction' by Spikes and Jie. Tribology Lett 2015;vol. 58(*nr. 16*). https://doi.org/10.1007/s11249-015-0481-x.
[26] Spikes H, Jie Z. Reply to the Comment by Scott Bair, Philippe Vergne, Punit Kumar, Gerhard Poll, Ivan Krupka, Martin Hartl, Wassim Habchi, Roland Larson on 'History, Origins and Prediction of Elastohydrodynamic Friction' by Spikes and Jie in Tribology Letters. Tribology Lett 2015;vol. 58(*nr. 17*). https://doi.org/10.1007/s11249-015-0483-8.
[27] Reynolds O. On the theory of lubrication and its applications to mr Beauchamp tower's experiments including an experimental determination of olive oil. Philos Trans R Soc 1886;177:157–234. https://doi.org/10.1098/rstl.1886.0005.
[28] Qiu Z, Yuen W, Tieu A. Mixed-Film Lubrication Theory and Tension Effects on Metal Rolling Processes. ASME J Tribology 1999;vol. 121:908–15. https://doi.org/10.1115/1.2834154.
[29] Patir N, Cheng HS. An average flow model for determining effects of three-dimensional roughness on partial hydrodynamic lubrication. J Lubr Techn 1978; Vol 100:12–7. https://doi.org/10.1115/1.3453103.
[30] Dowson D, Higginson G. Elasto-hydrodynamic lubrication - The Fundamentals of Roller and Gear Lubrication. Oxford: Pergamon Press; 1966. ISBN: 0-08-011472-5.
[31] Barus C. Isothermals, isopiestics and isometrics relative to viscosity. Am J Sicence 1893;vol. 45:87–96.
[32] Roelands CJA. Correlational aspects of the viscosity-temperature-pressure relationsip of lubricating oils (PhD Thesis). Technical University of Delft; 1966.
[33] Williams ML, Landel RF, Ferry JD. The Temperature Dependence of Relaxation Mechanisms in Amorphous Polymers and Other Glass-forming Liquids. J Am Chem Soc 1955;vol. 77:3701–7. https://doi.org/10.1021/ja01619a008.
[34] Bell JC, Kannel JW, Allen CM. The rheological behaviour of the lubricant in the contact zone of a rolling contact system, *ASME*. J Basic Eng 1964;vol. 86:423–32. https://doi.org/10.1115/1.3653124.
[35] Sutliffe MPF. Friction and Lubrication in Metal Rolling (PhD-thesis). University of Cambridge; 1989. https://doi.org/10.17863/CAM.14052.
[36] Gelinck E. Mixed Lubrication of Line Contacts (PhD-thesis). University of Twente; 1999.
[37] Poole RJ. The Deborah and Weissenberg number. Br Soc Rheol, Rheol Bull 2012; vol. 53:32–9.
[38] Spikes H. Basics of EHL foR Practical Application. Lubr Sci 2015;vol. 27:45–67. https://doi.org/10.1002/ls.1271.
[39] Blok H. Inverse Problems in Hydrodynamic Lubrication and Design for Lubricated Flexible Surfaces. Proc Int Symp Lubr Wear, Ed D Muster B Stern 1963:*1–151*.
[40] Montmitonnet P. Hot and cold strip rolling processes. Comput Methods Appl Mech Eng 2006;vol. 195:6604–25. https://doi.org/10.1016/j.cma.2005.10.014.
[41] Patir N, Cheng HS. Application of average flow model to lubrication between rough sliding surfaces. *1979* J Lubr Techn 1979;Vol. 101:220–30. https://doi.org/10.1115/1.3453329.
[42] Peklenik J. New Developments in Surface Characterization and Measurements by Means of Random Process Analysis. Proc Inst Mech Eng 1968;vol. 182:108–26. https://doi.org/10.1243/PIME_CONF_1967_182_309_02.
[43] Cassarini S. 2007. Modélisation du film lubrifiant dans la zone d'entrée, pour la lubrification par émulsion en laminage à froid, *PhD-thesis, ENSMP Paris*.
[44] van Liempt P. Workhardening and Substructural Geometry of Metals. J Mater Process Technol 1994;vol. 45:459–64. https://doi.org/10.1016/0924-0136(94)90382-4.
[45] Hill R. A theory of the yielding and plastic flow of anisotropicmetals. Proc R Soc Lond; Ser A 1948;vol. 193:281–97. https://doi.org/10.1098/rspa.1948.0045.
[46] Jacobs LJM, Atzema EH, Moerman J, de Rooij MB. Quantification of the influence of anisotropic plastic yielding on cold rolling force. J Mater Process Technol 2023; vol. 319:118055. https://doi.org/10.1016/j.jmatprotec.2023.118055.
[47] Hitchcock, J. 1935. Roll Neck Bearings*; Report of ASME Special Research Committee on Heavy-Duty Anti-Friction Bearings*.
[48] Johnson KL. Contact Mechanics. Cambridge University Press,; 1985.
[49] De Laurentis N, Kadiric A, Lugt P, Cann P. The influence of bearing grease composition on friction in rolling/sliding concentrated contacts. Tribol Int 2016; vol. 94:624–32. https://doi.org/10.1016/j.triboint.2015.10.012.
[50] Van Leeuwen H. The determination of the pressure–viscosity coefficient of a lubricant through an accurate film thickness formula and accurate film thickness measurements. Proc Inst Mech Eng Part J: J Eng Tribology 2009;vol. 223:1143–63. https://doi.org/10.1243/13506501JET504.
[51] Saeki K, Hashimoto Y. On the Oil Film Thickness in Cold Rolling of Thin Plate. J Jpn Soc Technol 1967;vol. 8:34–42.
[52] Azushima A. Determination of oil film thickness in rolling from the relationship between surface roughness of strip and roll. Bull JSME 1978;21(*159*):1402–7. https://doi.org/10.1299/jsme1958.21.1402.
[53] Cuperus RS, ten Napel WE, Neumann WH, Smits RPJM. Measurements of film thickness and friction in cold rolling. Trans Mech Eng 2000;vol. 24(*No. 1*):59–65.
[54] Aggarwal BB, Wilson WRD. Thermal effects in hydrodynamically lubricated strip rolling. Proc 5th Leeds-Lyon Symp Tribology, I Mech E Pap X 1978:351–9.
[55] Jacobs LJM, van Dam KNH, Wentink DJ, de Rooij MB, van der Lugt J, Schipper DJ, Hoefnagels JPM. Effect of asymmetric material entrance on lubrication in cold rolling. Tribology Int 2022;vol. 175:107810. https://doi.org/10.1016/j.triboint.2022.107810.
[56] Evans C. Measurement and Mapping of the Rheological Properties of Elastohydrodynamic Lubricants (Phd-thesis). University of Cambridge,; 1983.
[57] Yuen WYD, Popelianski Y, Prouten M. Variations of friction in the roll bite and their effects on cold strip rolling. *Proc 37th Conf Mech Work Steel Process* 1996: 47–54.
[58] Shiraishi T, Yamamoto H, Hashimoto J, Niitome T. Characteristics of cold rolling in consideration of negative forward slip ratio. J Jpn Soc Technol Plast 1995;vol. 36 (412). 457-452.
[59] Liu HC, Zhang BB, Bader N, Venner CH, Poll G. Simplified traction prediction for highly loaded rolling/sliding EHL contacts. Tribology Int 2020;vol. 148:106335. https://doi.org/10.1016/j.triboint.2020.106335.
[60] Faghri A, Zhang Y. Transport Phenomena in Multiphase Systems. Elsevier Academic Press,; 2006. *ISBN 978-0-12-370610-2*.
[61] Blumm J, Lindemann A. Characterization of the thermophysical properties of molten polymers and liquids using the flash technique. High Temp - High Press 2003;vol. 35/36:627–32. https://doi.org/10.1068/htjr144.
[62] Liu HC, Zhang BB, Bader N, Guo F, Poll G, Yang P. Crucial role of solid body temperature on elastohydrodynamic film thickness and traction. Tribology Int 2019;vol. 131:386–97. https://doi.org/10.1016/j.triboint.2018.11.006.
[63] Sheu S, Wilson WRD. Mixed lubrication of strip rolling. Tribology Trans 1994;vol. 37:483–93. https://doi.org/10.1080/10402009408983321.
[64] Wilson WRD, Chang D. Low speed mixed lubrication of bulk metal forming processes. J Tribol 1996;vol. 118:83–9. https://doi.org/10.1115/1.2837096.
[65] Christensen H. Stochastic models for hydrodynamic lubrication of rough surfaces. Proc Inst Mech Eng 1969;vol. 184:1013–26. https://doi.org/10.1243/PIME_PROC_1969_184_074_02.
[66] Shigaki Y, Nakhoul R, Montmitonnet P. Numerical treatments of slipping/no-slip zones in cold rolling of thin sheets with heavy roll deformation. Lubricants 2015; vol. 3:113–31. https://doi.org/10.3390/lubricants3020113.